



HAL
open science

Symbolic Monte Carlo method applied to the identification of radiative properties of a heterogeneous material

Yassine Maanane, Maxime Roger, Agnès Delmas, Mathieu Galtier, Frédéric André

► **To cite this version:**

Yassine Maanane, Maxime Roger, Agnès Delmas, Mathieu Galtier, Frédéric André. Symbolic Monte Carlo method applied to the identification of radiative properties of a heterogeneous material. *Journal of Quantitative Spectroscopy and Radiative Transfer*, 2020, 249, pp.107019. 10.1016/j.jqsrt.2020.107019 . hal-02613374

HAL Id: hal-02613374

<https://hal.science/hal-02613374v1>

Submitted on 20 May 2020

HAL is a multi-disciplinary open access archive for the deposit and dissemination of scientific research documents, whether they are published or not. The documents may come from teaching and research institutions in France or abroad, or from public or private research centers.

L'archive ouverte pluridisciplinaire **HAL**, est destinée au dépôt et à la diffusion de documents scientifiques de niveau recherche, publiés ou non, émanant des établissements d'enseignement et de recherche français ou étrangers, des laboratoires publics ou privés.

Symbolic Monte Carlo method applied to the identification of radiative properties of a heterogeneous material.

Yassine Maanane^a, Maxime Roger^{a,*}, Agnès Delmas^a, Mathieu Galtier^a,
Frédéric André^a

^a*Univ Lyon, CNRS, INSA-Lyon, Université Claude Bernard Lyon 1, CETHIL UMR5008,
F-69621 Villeurbanne, France*

Abstract

A Symbolic Monte Carlo method (SMC) is applied to the identification of radiative properties of a heterogeneous semitransparent insulating material from measurements of directional-hemispherical transmittance and reflectance at room temperature. The polynomials obtained with SMC allow the development of a complete inverse analysis which determines if the inverse problem solution exists, is unique and stable. Moreover, the numerical efficiency of the absorption and scattering coefficients identification is improved since the radiative transfer equation is only solved once in the overall inverse iterative procedure.

Keywords: Radiative Transfer, Symbolic Monte Carlo (SMC), Polynomials, Radiative properties, Identification, Insulating materials

1. Introduction

2 Inverse problems in radiative transfer concern many applications including
3 the characterization of complex media (porous or fibrous [1, 2], combustion di-
4 agnosis [3], medical imaging [4, 5], etc.). Identification methods combine spec-
5 troscopic measurements with simulations based on radiative models, such as
6 the radiative transfer equation (RTE), in order to infer parameters such as

*Corresponding author

Email address: maxime.roger@insa-lyon.fr (Maxime Roger)

7 radiative properties, temperature or species concentrations. For instance, spec-
8 tral measurements of transmitted and reflected fluxes in different configurations
9 (bidirectional, directional-hemispherical, hemispherical-hemispherical ...) can
10 be used to identify the effective scattering and absorption properties of various
11 media [6, 7, 8]. In these approaches, inversion is performed by using an itera-
12 tive procedure, where at each step, direct computations and measurements are
13 compared.

14 In the frame of inverse radiative transfer problems, Symbolic Monte Carlo
15 methods (SMC) turns out to be a powerful and efficient tool for inverse anal-
16 ysis and to improve the efficiency of identification method. The principle of
17 SMC consists in retaining some parameters as symbols in a Monte Carlo simu-
18 lation, in order to express the observable as a simple and unbiased function of
19 those symbolic parameters [9]. The observable is therefore estimated all over
20 the parameter space, which is valuable for inversion analysis purpose. SMC
21 (initially labeled inverse Monte Carlo method) was introduced by Dunn [10]
22 and investigated for inverse problems in radiative transfer in [10, 11]. Dunn [10]
23 identified the scattering albedo in an inhomogeneous medium assuming isotropic
24 scattering. The approach was extended by Subramaniam *et al.* [11] to iden-
25 tify the scattering albedo and the asymmetry factor of the phase function in
26 an anisotropically scattering medium. However, the identification of absorption
27 and scattering coefficients was impossible in [10, 11] as the analysis required the
28 knowledge of the optical thickness. Galtier *et al.* [12] circumvented this diffi-
29 culty by the use of null-collisions method [13] to express a radiative quantity as
30 a polynomial of absorption and scattering coefficients.

31 In this work, SMC algorithms presented in [12] are developed within the
32 frame of inverse radiative transfer. A complete SMC framework for the iden-
33 tification of absorption and scattering coefficients of heterogeneous semitrans-
34 parent materials from measurements of directional-hemispherical transmittance
35 and reflectance is proposed. An inverse analysis based on SMC is developed
36 and advantages related to the use of SMC are highlighted: from inverse analysis
37 (discussion on the well or ill-posed character of the problem), up to the fast

38 experimental identification of radiative properties, including experimental and
39 numerical errors. The whole method is illustrated here in the case of a low
40 density fibrous medium but the approach is not restricted to this material and
41 can be used for other types of heterogeneous media.

42 The paper is structured as follows. In the second section, experimental setup
43 and spectroscopic measurements are presented. In the third section, details
44 of the proposed Symbolic approach are given: SMC algorithm that allows to
45 obtain simple polynomial forms of directional-hemispherical transmittance and
46 reflectance as function of absorption and scattering coefficients is presented.
47 These polynomials are then used to determine the nature (well or ill-posed) of
48 the inverse problem, including experimental and numerical errors in the analysis.
49 Finally, in the last section, inversion based on these polynomials is carried out
50 to retrieve absorption and scattering coefficients of a Quartzel sample.

51 **2. Sample description and experimental measurements**

52 *2.1. Sample description*

53 The medium considered is a Quartzel low density felt (Saint-Gobain Quartz)
54 sample. It is used as insulation material for aircraft engines or furnace closures.
55 It is also used as a support for catalysts in domestic and industrial catalytic
56 heaters. Felts provided by Saint-Gobain have an estimated thickness of 11 *mm*
57 when not compressed, which corresponds, according to the material brochure, to
58 an areal weight of 100 $g.m^{-2}$ and an estimated density of [10; 20] $kg.m^{-3}$. Low
59 density felts are produced from 9 microns pure fused quartz fibers (Quartzel
60 wool) with a constant diameter along their length. They are randomly oriented
61 in parallel planes and are impregnated with an organic binder (PolyVinyl Alco-
62 hol). In this work, anisotropy of the sample was not assessed as bi-directional
63 measurements of transmittance and reflectance were not performed. Size dis-
64 tribution of fibers in the medium can be modeled as a normal distribution with
65 9 μm mean and 2 μm variance. Porosity of the studied sample is higher than

66 95% (volume fraction of fibers lower than 5%). A picture of the felt is shown in
67 Figure 1.

68 The studied sample is cylindrical with 24 mm diameter and 4 mm width.
69 The sample is constrained between two ZnSe windows with a multilayer Broad
70 Band Anti Reflectance coating in the spectral region $[830; 3330]$ cm^{-1} , all in a
71 3D-printed sample holder specifically designed for the current apparatus.

72 2.2. Experimental setup, measurements and uncertainty evaluation

73 Spectroscopic measurements were carried out using a Bruker IFS 66v/S
74 Fourier-transform infrared (FTIR) spectrometer. The incident radiative flux
75 is provided by a Globar source for mid-infrared (MIR) spectroscopy (spectral
76 range of $[666; 5000]$ cm^{-1} equivalent to $[2; 15]$ μm). An infragold A562G inte-
77 grating sphere provided with a DTGS detector allows directional-hemispherical
78 transmittance and reflectance measurements as illustrated in figure 2. The total
79 diameter of the sphere is 75 mm and the inner wall of the sphere is coated with a
80 layer of diffuse reflecting gold that reflects the incoming light several times and
81 scatters it uniformly around the interior of the sphere (the integrating sphere
82 ensures a homogeneous spatial light intensity distribution). The apparatus is
83 permanently flushed with dry air with low CO_2 and H_2O concentration to re-
84 duce atmospheric absorption in the following spectral ranges: $[3389; 4000]$ cm^{-1} ,
85 $[2222; 2398]$ cm^{-1} , $[1250; 2083]$ cm^{-1} and $[581; 757]$ cm^{-1} . Purging the integrat-
86 ing sphere also ensures a constant concentration of atmospheric constituents
87 over time.

88 Experimental transmittance and reflectance spectra for the sample described
89 above are provided as a function of wavenumbers η [cm^{-1}] and wavelengths
90 $\lambda = 10^4/\eta$ [μm] in figure 3. Measurements of transmittance and reflectance are
91 performed, at ambient temperature in the spectral range $[700; 3700]$ cm^{-1} . One
92 spectrum is the result of 50 scans of the interferometer at a spectral resolution
93 of 16 cm^{-1} , and measurements illustrated in figure 3 are obtained by averaging
94 100 spectra performed on the same sample over a week period. Transmittance
95 (respectively reflectance) is the ratio of transmitted (respectively reflected) ra-

96 diative heat flux by the sample to the incident one called reference. Spectra
 97 are obtained from two consecutive measurements. Because it is necessary to
 98 perform these two successive steps, atmospheric conditions vary between the
 99 two measurements. Despite all precautions to reduce effects of CO₂ absorp-
 100 tion, its concentration still varied during time which induced absorption bands
 101 mainly near $\eta = 2350 \text{ cm}^{-1}$ (see colored band in figure 3). Transmittance and
 102 reflectance measurements in this absorption band will not be taken into account
 103 in the identification process.

104 In order to estimate the uncertainty of FTIR spectroscopic measurements,
 105 one must take into account a large number of sources that may affect the in-
 106 terpretation of the spectrum. Sources of errors can be a change of ambient
 107 temperature, a variation of the concentration of atmospheric absorbents like
 108 water vapor and carbon dioxide, an inefficient cooling of the MIR source, a
 109 heating of the source's aperture, a loss of efficiency of optics, a non-linear re-
 110 sponse of detector, interreflections involving the sample, etc. These errors lead
 111 to experimental uncertainties. Measurement uncertainty is defined as:

$$U = k \sqrt{\sum_{i=1}^{i=n} u_{b,i}^2 + u_{rand}^2} \quad (1)$$

112 where $u_{b,i}$ are individual sources of uncertainty and u_{rand} is the uncertainty
 113 related to random errors. The uncertainties are wavelength-dependent, therefore
 114 they must be computed for the specific wavelength and the specific sample.
 115 Most of errors are dependent and it is difficult to quantify their associated
 116 uncertainties. A first approach to estimate the measurements uncertainties is
 117 to only take into account the effects of the detector internal noise (u_b) and
 118 to consider that all other error sources are random (u_{rand}). In figures 3a and
 119 3b, error bars were obtained for each wavenumber using the detector internal
 120 noise and the standard-deviation of 100 measurements performed over a week
 121 period. The coverage factor k was taken equal to 2 in order to have an extended
 122 absolute uncertainty with a confidence interval of 95%. A quasi-similar approach
 123 was proposed by [14] for the evaluation of emissivity from transmittance and

124 reflectance measurements at ambient temperature. In the present work, absolute
125 experimental uncertainties were estimated at 0.01.

126 **3. Identification of absorption and scattering coefficients based on** 127 **SMC Analysis**

128 *3.1. Model*

129 A schematic representation of the problem considered is given in figure 4.
130 The medium (Quartzel sample) noted Δ is at ambient temperature. An incident
131 beam of intensity $I_{0,\eta}$ in the \mathbf{u}_0 direction crosses the surface S_0 . We define the
132 surface S_R (respectively S_T) corresponding to the abscissa $x = 0$ mm (respec-
133 tively $x = 4$ mm) for which spectral reflectance (respectively transmittance) is
134 estimated.

135 The Radiative Transfer Equation (RTE) in an equivalent homogeneous ab-
136 sorbing and scattering medium is considered for modeling radiative transfer in
137 the fibrous material. Bidirectional measurements need to be performed if in-
138 formation about anisotropy is expected. Consequently, phase function cannot
139 be identified from directional-hemispherical transmittance and reflectance, and
140 may be assumed either isotropic or modeled by the Delta-Eddington (DE) ap-
141 proximation. In DE case, the phase function asymmetry factor g_η is included
142 in the reduced scattering coefficient $\sigma'_\eta = \sigma_\eta(1 - g_\eta)$ where σ_η is the scattering
143 coefficient.

144 RTE in homogeneous media has been chosen to model radiative transfer in
145 Quartzel sample because of its low density, its high porosity and the random
146 orientation of its fibers. The boundary conditions are given by $I_\eta(\mathbf{x}_0, \mathbf{u}_0) =$
147 $I_{0,\eta}$ if $\mathbf{x}_0 \in S_0$, 0 elsewhere. Using this model, absorption coefficient κ_η and
148 scattering coefficient σ_η need to be identified.

149 *3.2. Standard forward null-collision Monte Carlo algorithm*

150 A forward null-collision Monte Carlo algorithm is applied to simulate radia-
151 tive transfer in the medium. Null-collision algorithms [13] are needed to express

152 the radiative intensity as a polynomial of κ_η and σ_η as shown in [12]. The
 153 formulations, based on the integral form of the RTE, of transmitted directional-
 154 hemispherical transmittance T_η and reflectance R_η are given by the following
 155 equations:

$$\begin{aligned}
 T_\eta &= \frac{\int_{S_0} I_{0,\eta} dS \times \Gamma_\eta\left((\mathbf{x}_0, \mathbf{u}_0) \rightarrow (\mathbf{x}_T, \mathbf{u}_T)\right)}{\int_{S_0} I_{0,\eta} dS} \\
 R_\eta &= \frac{\int_{S_0} I_{0,\eta} dS \times \Gamma_\eta\left((\mathbf{x}_0, \mathbf{u}_0) \rightarrow (\mathbf{x}_R, \mathbf{u}_R)\right)}{\int_{S_0} I_{0,\eta} dS}
 \end{aligned} \tag{2}$$

156 where \mathbf{x}_T (or \mathbf{x}_R) is a position on the surface S_T (or S_R) and \mathbf{u}_T (or \mathbf{u}_R)
 157 is the optical path direction when it outgoes the surface S_T (or S_R). Γ is a
 158 dimensionless quantity and can be interpreted as a transmission function from
 159 the incident beam to the outbound surface. The determination of the transmis-
 160 sion function Γ_η is based on a forward Monte Carlo algorithm and is estimated
 161 recursively using the following expression:

$$\begin{aligned}
 &\Gamma_\eta\left((\mathbf{x}_0, \mathbf{u}_0) \rightarrow (\mathbf{x}_T, \mathbf{u}_T)\right) \\
 &= \int_0^\infty \widehat{\beta}_\eta \exp(-\widehat{\beta}_\eta l_1) dl_1 \times \left(H(\mathbf{x}_1 \in \Delta) \left[\frac{\kappa_\eta}{\widehat{\beta}_\eta} \times 0 + \frac{\sigma_\eta}{\widehat{\beta}_\eta} \int_{4\pi} \frac{1}{4\pi} \Gamma_\eta(\mathbf{x}_1, \mathbf{u}_1) d\mathbf{u}_1 \right. \right. \\
 &\quad \left. \left. + \frac{\widehat{\beta}_\eta - \kappa_\eta - \sigma_\eta}{\widehat{\beta}_\eta} \Gamma_\eta(\mathbf{x}_1, \mathbf{u}_1 = \mathbf{u}_0) \right] + H(\mathbf{x}_1 \notin \Delta) H(\mathbf{x}_1 \rightarrow S_T) \right)
 \end{aligned} \tag{3}$$

162 where $H(C)$ is the Heaviside function (equal to 1 if condition C is satisfied),
 163 $\widehat{\beta}_\eta = \kappa_\eta + \sigma_\eta + \gamma_\eta$ is the extinction coefficient including null-collisions [13] and
 164 γ_η is the null-collision coefficient. This expression is also valid for reflectance by
 165 changing index T with R .

166 Standard forward null-collisions Monte-Carlo algorithms perform a large
 167 number N_{MC} of independent optical path realizations indexed i . Free-paths
 168 are sampled according to the probability density $\widehat{p}_L(l) = \widehat{\beta}_\eta \exp(-\widehat{\beta}_\eta l)$. Null-
 169 collisions coefficient γ_η introduces pure-forward scattering events. The value of

170 $\widehat{\beta}_\eta$ determines the upper bound of the real extinction coefficient $\beta_\eta = \kappa_\eta + \sigma_\eta$
 171 over which the functional will be defined [13].

172 Using this algorithm, the i -th optical path realization starts with the sam-
 173 pling of a location \mathbf{x}_0 in S_0 according to a uniform probability density function
 174 $\frac{1}{S_0}$. A free path $l_{1,i}$ is then sampled according to $\widehat{p}_L(l_{1,i})$ and a new position
 175 $\mathbf{x}_{1,i} = \mathbf{x}_0 + l_{1,i}\mathbf{u}_0$ is deduced. At this point, two approaches can be used for
 176 the standard algorithm.

177 In the most usual approach, a step is required to statistically determine which
 178 type of event occurs: an absorption with probability given by $\frac{\kappa_\eta}{\widehat{\beta}_\eta}$, a scattering
 179 given by the probability $\frac{\sigma_\eta}{\widehat{\beta}_\eta}$ or a null-collision with probability $\frac{\widehat{\beta}_\eta - \kappa_\eta - \sigma_\eta}{\widehat{\beta}_\eta}$.
 180 However, an absorption event will always lead to a null Monte Carlo weight since
 181 the quantities of interest are transmittance and reflectance, not absorptance (Eq
 182 3). Therefore, an energy partitioning approach is applied in this work as in [15].
 183 Following this approach, absorption attenuation is still accounted for in the
 184 sampling of extinction free paths according to Beer's law $\widehat{\beta} \exp(-\widehat{\beta}L)$, but the
 185 statistical determination of a collision will only concern scattering and null-
 186 collision. A probability $P_{s,\eta}$ for scattering, and $P_{n,\eta} = 1 - P_{s,\eta}$ for null-collision,
 187 is therefore introduced in the algorithm. Eq 3 becomes:

$$\begin{aligned}
 & \Gamma_\eta\left(\left(\mathbf{x}_0, \mathbf{u}_0\right) \rightarrow \left(\mathbf{x}_T, \mathbf{u}_T\right)\right) \\
 &= \int_0^\infty \widehat{\beta}_\eta \exp(-\widehat{\beta}_\eta l_1) dl_1 \times \left(H(\mathbf{x}_1 \in \Delta) \left[P_{s,\eta} \frac{\sigma_\eta}{\widehat{\beta}_\eta P_{s,\eta}} \int_{4\pi} \frac{1}{4\pi} \Gamma_\eta(\mathbf{x}_1, \mathbf{u}_1) d\mathbf{u}_1 \right. \right. \\
 & \quad \left. \left. + (1 - P_{s,\eta}) \frac{\widehat{\beta}_\eta - \kappa_\eta - \sigma_\eta}{\widehat{\beta}_\eta (1 - P_{s,\eta})} \Gamma_\eta(\mathbf{x}_1, \mathbf{u}_1 = \mathbf{u}_0) \right] + H(\mathbf{x}_1 \notin \Delta) H(\mathbf{x}_1 \rightarrow S_T) \right)
 \end{aligned} \tag{4}$$

188 where $P_{s,\eta}$ can be expressed as:

$$P_{s,\eta} = \frac{\sigma_\eta}{\sigma_\eta + \gamma_\eta} = \frac{\sigma_\eta}{\widehat{\beta}_\eta - \kappa_\eta} \tag{5}$$

189 Consequently, at position $\mathbf{x}_{1,i}$, scattering and null-collision events are sampled
 190 according to $P_{s,\eta}$ and $1 - P_{s,\eta}$. If scattering occurs at position $\mathbf{x}_{1,i}$, a new

191 direction of propagation \mathbf{u}_1 is sampled according to $\frac{1}{4\pi}$, and the transmis-
 192 sion function Γ is multiplied by $\frac{\sigma_\eta}{\widehat{\beta}_\eta P_{s,\eta}}$. If a null-collision occurs, direction of
 193 propagation \mathbf{u}_1 is equal to the previous one \mathbf{u}_0 as null-collisions correspond
 194 to pure forward-scattering, and the transmission function Γ is multiplied by
 195 $\frac{\widehat{\beta}_\eta - \kappa_\eta - \sigma_\eta}{\widehat{\beta}_\eta(1 - P_{s,\eta})}$. A new free path $l_{2,i}$ is then sampled. The algorithm loops until
 196 the optical path exits the medium. If the optical path exits the domain through
 197 the surface S_T , transmittance is implemented (the associated Heaviside distribu-
 198 tion corresponding to the estimation of directional-hemispherical transmittance
 199 is $H_{T,i} = 1$, and $H_{R,i} = 0$). On the opposite, if the outbound surface is S_R ,
 200 reflectance is implemented (the associated Heaviside distribution correspond-
 201 ing to the estimation of directional-hemispherical reflectance is $H_{R,i} = 1$, and
 202 $H_{T,i} = 0$).

203 For illustration, let us assume that along the i -th Monte Carlo path sample, the
 204 following events occur: one scattering, two null-collisions and another scattering
 205 before the optical path exits the medium. According to equation 4 and using
 206 the energy partitioning approach, the associated Monte Carlo weight for the
 207 estimation of transmittance is expressed in this case by:

$$w_{T,i} = \frac{\sigma_\eta}{\widehat{\beta}_\eta P_{s,\eta}} \left\{ \frac{\widehat{\beta}_\eta - \kappa_\eta - \sigma_\eta}{\widehat{\beta}_\eta(1 - P_{s,\eta})} \left[\frac{\widehat{\beta}_\eta - \kappa_\eta - \sigma_\eta}{\widehat{\beta}_\eta(1 - P_{s,\eta})} \left(\frac{\sigma_\eta}{\widehat{\beta}_\eta P_{s,\eta}} H_{T,i} \right) \right] \right\} \quad (6)$$

208 which, given the expression of $P_{s,\eta}$ (Eq. 5), simplifies into:

$$w_{T,i} = \left(\frac{\widehat{\beta}_\eta - \kappa_\eta}{\widehat{\beta}_\eta} \right)^4 H_{T,i} \quad (7)$$

209 In general, Monte Carlo weights for the estimation of transmittance and re-
 210 flectance can be expressed as:

$$w_{T,i} = \left(\frac{\widehat{\beta}_\eta - \kappa_\eta}{\widehat{\beta}_\eta} \right)^{N_{sca,i} + N_{nc,i}} H_{T,i} \quad (8)$$

211 where $N_{sca,i}$ and $N_{nc,i}$ are the number of scattering and null-collision events
 212 that occurred along the i -th optical path.

213 *3.3. Symbolic Monte Carlo algorithm*

214 Radiative quantities can be expressed using SMC as bivariate polynomials
 215 of absorption coefficient κ_η and scattering coefficient σ_η [12]:

$$\begin{aligned} T_\eta(\kappa_\eta, \sigma_\eta) &= \sum_{j=0}^{\infty} \sum_{k=0}^{\infty} a_{jk} \kappa_\eta^j \sigma_\eta^k \\ R_\eta(\kappa_\eta, \sigma_\eta) &= \sum_{j=0}^{\infty} \sum_{k=0}^{\infty} b_{jk} \kappa_\eta^j \sigma_\eta^k \end{aligned} \quad (9)$$

216 The standard forward null-collision Monte Carlo algorithm described in previous
 217 section can be applied only if numerical values are affected to the absorption
 218 and scattering coefficients. In SMC, if κ_η and σ_η are kept under their symbolic
 219 form, and consequently the probability of scattering event $P_{s,\eta} = \frac{\sigma_\eta}{\widehat{\beta}_\eta - \kappa_\eta}$ (and
 220 $1 - P_{s,\eta}$ for null-collision) is unknown. The choice of $P_{s,\eta}$ becomes therefore
 221 arbitrary [12] (this arbitrary probability is denoted \widetilde{P}_s). In this work, \widetilde{P}_s is
 222 chosen equal to 0.5 for all wavenumbers. The choice of this arbitrary probability
 223 has an impact on the variance which is analyzed in [Appendix A](#).
 224 Now, if we assume that along the i -th Monte Carlo path sample, one scattering,
 225 two null-collisions and another scattering events occur before the optical path
 226 exits the medium (i.e., $N_{nc,i} = 2$ and $N_{sca,i} = 2$), the associated Monte Carlo
 227 weight is expressed by:

$$w_{SMC,T,i} = \frac{\sigma_\eta}{\widehat{\beta}_\eta \widetilde{P}_s} \left\{ \frac{\widehat{\beta}_\eta - \kappa_\eta - \sigma_\eta}{\widehat{\beta}_\eta (1 - \widetilde{P}_s)} \left[\frac{\widehat{\beta}_\eta - \kappa_\eta - \sigma_\eta}{\widehat{\beta}_\eta (1 - \widetilde{P}_s)} \left(\frac{\sigma_\eta}{\widehat{\beta}_\eta \widetilde{P}_s} H_{T,i} \right) \right] \right\} \quad (10)$$

which can be rewritten as a polynomial:

$$w_{SMC,T,i} = \left(\frac{\sigma_\eta}{\widehat{\beta}_\eta \widetilde{P}_s} \right)^2 \left(\frac{\widehat{\beta}_\eta - \kappa_\eta - \sigma_\eta}{\widehat{\beta}_\eta (1 - \widetilde{P}_s)} \right)^2 H_{T,i} \quad (11)$$

More generally, the total contribution of the i -th optical path with $N_{nc,i}$ null-
 collision events and $N_{sca,i}$ scattering events is written in the general case:

$$w_{SMC,T,i} = \left(\frac{\widehat{\beta}_\eta - \kappa_\eta - \sigma_\eta}{\widehat{\beta}_\eta (1 - \widetilde{P}_s)} \right)^{N_{nc,i}} \left(\frac{\sigma_\eta}{\widehat{\beta}_\eta \widetilde{P}_s} \right)^{N_{sca,i}} H_{T,i} \quad (12)$$

228 In order to introduce the symbolic MC weight $a_{jk,i}$ of the polynomial coefficients
 229 (associated to the i -th optical path), Eq. 12 is rewritten as:

$$w_{SMC,T,i} = \sum_{j=0}^{\infty} \sum_{k=0}^{\infty} \left(\frac{\widehat{\beta}_{\eta} - \kappa_{\eta} - \sigma_{\eta}}{\widehat{\beta}_{\eta}(1 - \widetilde{P}_s)} \right)^j \left(\frac{\sigma_{\eta}}{\widehat{\beta}_{\eta}\widetilde{P}_s} \right)^k a_{jk,i} \quad (13)$$

230 where $a_{jk,i}$ is a non-zero coefficient only if $j = N_{nc,i}$ and $k = N_{sca,i}$:

$$a_{jk,i} = \delta_{j,N_{nc,i}} \delta_{k,N_{sca,i}} H_{T,i} \quad (14)$$

231 where δ is the Kronecker symbol. Directional-hemispherical transmittance and
 232 reflectance are expressed as polynomial of absorption and scattering coefficients
 233 according to:

$$\begin{aligned} T_{\eta} &\simeq \sum_{j=0}^{\infty} \sum_{k=0}^{\infty} \overline{a_{jk}} \left(\frac{\widehat{\beta}_{\eta} - \kappa_{\eta} - \sigma_{\eta}}{\widehat{\beta}_{\eta}(1 - \widetilde{P}_s)} \right)^j \left(\frac{\sigma_{\eta}}{\widehat{\beta}_{\eta}\widetilde{P}_s} \right)^k \\ R_{\eta} &\simeq \sum_{j=0}^{\infty} \sum_{k=0}^{\infty} \overline{b_{jk}} \left(\frac{\widehat{\beta}_{\eta} - \kappa_{\eta} - \sigma_{\eta}}{\widehat{\beta}_{\eta}(1 - \widetilde{P}_s)} \right)^j \left(\frac{\sigma_{\eta}}{\widehat{\beta}_{\eta}\widetilde{P}_s} \right)^k \end{aligned} \quad (15)$$

234 where coefficients $\overline{a_{jk}}$ and $\overline{b_{jk}}$ are estimated with SMC using the following ap-
 235 proximations:

$$\begin{aligned} \overline{a_{jk}} &\approx \frac{1}{N_{MC}} \sum_{i=1}^{N_{MC}} a_{jk,i} \\ \overline{b_{jk}} &\approx \frac{1}{N_{MC}} \sum_{i=1}^{N_{MC}} b_{jk,i} \end{aligned} \quad (16)$$

236 A flowchart of the SMC algorithm is shown in figure 5. At each optical path
 237 $i \in \{1, \dots, N_{MC}\}$, the number of scattering $N_{sca,i}$ and null-collisions events
 238 $N_{nc,i}$ is counted in order to calculate the coefficients $a_{jk,i}$ and $b_{jk,i}$ according to
 239 Eq. 14. Once the N_{MC} optical paths have been generated, the coefficients $\overline{a_{jk}}$
 240 and $\overline{b_{jk}}$ are estimated according to Eq. 16.

241 R_{η} and T_{η} are expressed as polynomial functions of σ_{η} and $\widehat{\beta} - \kappa_{\eta} - \sigma_{\eta}$, but
 242 it is possible to re-express R_{η} and T_{η} as a polynomials of κ_{η} and σ_{η} since the
 243 value of $\widehat{\beta}$ is fixed in the SMC procedure.

244 It should be emphasized that all the estimated polynomial coefficients $\overline{a_{jk}}$
 245 and $\overline{b_{jk}}$ are independent of the wavenumbers. This is a direct consequence of the
 246 choice of a constant arbitrary probability \widetilde{P}_s . If \widetilde{P}_s was wavenumber-dependent,
 247 as many polynomials as wavenumbers would be needed. Here, one single SMC
 248 calculation is sufficient to express T_η and R_η as functions of κ_η and σ_η , and only
 249 those two polynomials are used over the full spectrum.

250 3.4. Inverse analysis based on SMC polynomials

251 All results presented in the following subsections were obtained using $N_{MC} =$
 252 10^6 , $\widehat{\beta}_\eta = 20 \text{ cm}^{-1}$ and $\widetilde{P}_s = 0.5$. S_0 is a disk with 12mm diameter. Without
 253 any *a priori* information about scattering inside the considered material, the
 254 choice of $\widetilde{P}_s = 0.5$ represents a good compromise to obtain a satisfactory accu-
 255 racy for both thin and thick scattering optical thickness (as discussed in [12]).
 256 Here, with $\widetilde{P}_s = 0.5$, the average relative standard deviation is 1.1% for trans-
 257 mittance and 1.0% for reflectance (maximum relative standard-deviation is 2.1%
 258 for transmittance and 2.6% for reflectance) and allows the identification of ra-
 259 diative properties in most part of the spectrum. The influence of the choice of
 260 $\widetilde{P}_s = 0.5$ on the standard-deviation is discussed in [Appendix A](#).

261 The functional obtained with SMC allows to efficiently estimate the quanti-
 262 ties (since one simulation is required), T_η and R_η , all over the parameter space:
 263 $\kappa_\eta \in [0, 10]$ and $\sigma_\eta \in [0, 10]$. It is therefore possible to plot isovalues of trans-
 264 mittance and reflectance as functions of absorption and scattering coefficients
 265 as depicted in [Figure 6](#).

266 According to the RTE model, isolines that lead to given values of T_η and
 267 R_η are displayed for an infinity of couples $(\kappa_\eta, \sigma_\eta)$. An isoline gives the range
 268 of possible values of κ_η and σ_η that reproduce the measured transmittance or
 269 reflectance. For example, the isoline $T_\eta = 0.3$ in [figure 6a](#) gives the possible
 270 values of absorption and scattering coefficients $\kappa_\eta \in [0; 3] \text{ cm}^{-1}$ and $\sigma_\eta \in [0; 8.7]$
 271 cm^{-1} that are compatible with this particular value of T_η .

272 From those isolines, it is possible to determine if the solution of the inverse
 273 problem exists, and if it is unique. The first case considered in [figure 7a](#) cor-

274 responds to the measured values $T_\eta = 0.03$ and $R_\eta = 0.18$ at $\eta = 900 \text{ cm}^{-1}$.
 275 In figure 7a, the isoline corresponding to $T_\eta = 0.03$ is depicted in red lines,
 276 and the isoline corresponding to $R_\eta = 0.18$ is depicted in green lines. This
 277 graphical method, also called the contour intersection approach [16], allows to
 278 determine the absorption and scattering coefficients that are solutions of the
 279 inverse problem by plotting the isolines corresponding to the measurements of
 280 T_η and R_η . Intersections represent values of κ_η and σ_η that reproduce the
 281 measured transmittance and reflectance according to the RTE model. If no in-
 282 tersection appears, then the solution of the inverse problem does not exist. If
 283 several intersections are observed, then the solution exists, but is not unique.
 284 In figure 7a, only one intersection is obtained in the parameter space, which
 285 shows that the solution exists and is unique: $\kappa_\eta = 3.90 \text{ cm}^{-1}$ and $\sigma_\eta = 7.44$
 286 cm^{-1} . The same conclusion can be drawn in figure 7b where measured values
 287 $T_\eta = 0.01$ and $R_\eta = 0.08$ at $\eta = 1189 \text{ cm}^{-1}$ are considered: $\kappa_\eta = 7.62 \text{ cm}^{-1}$
 288 and $\sigma_\eta = 4.92 \text{ cm}^{-1}$.

289 However, even if the solution exists and is unique, the inverse problem
 290 can be ill-posed if the solution is unstable according to Hadamard's defini-
 291 tion. Consequently, the feasibility of the identification cannot be ensured as
 292 long as experimental and numerical errors are not taken into account. Using
 293 SMC polynomials, experimental and numerical errors can be easily included
 294 in the analysis as illustrated in figure 7. Measurement and numerical (SMC
 295 standard-deviations) errors are introduced by plotting the isolines correspond-
 296 ing to $T_\eta + \varepsilon(T_\eta)$, $T_\eta - \varepsilon(T_\eta)$, $R_\eta + \varepsilon(R_\eta)$ and $R_\eta - \varepsilon(R_\eta)$ where ε is the total
 297 error at wavenumber η . The colored (orange) polygons and filled plots in fig-
 298 ure 7 represent the range of possible κ_η and σ_η that reproduce the measured
 299 transmittance and reflectance according to the RTE model, with respect to the
 300 estimated experimental and numerical uncertainties.

301 In figure 7a, the estimated relative uncertainties of 30% for transmittance
 302 and 4% for reflectance are taken into account at $\eta = 900 \text{ cm}^{-1}$. Absorption
 303 coefficients range in the intervals $[3.46; 4.50] \text{ cm}^{-1}$ (relative error lower than
 304 15.4%) and scattering coefficients range in $[6.57; 8.61] \text{ cm}^{-1}$ (relative error lower

305 than 15.8%). There may be noise amplification, but the domain within which
 306 the couple $(\kappa_\eta, \sigma_\eta)$ is located remains of limited size. In figure 7b, errors are
 307 taken into account at $\eta = 1189 \text{ cm}^{-1}$ (98% for transmittance and 10% for
 308 reflectance). Possible solutions of the inverse problem are not bounded as all
 309 absorption and scattering coefficients that are respectively greater than 6.25
 310 cm^{-1} and 3.78 cm^{-1} (filled bold polygon) belong to the parameter space region
 311 where transmittance is $0.01 \pm 98\%$ and reflectance is $0.09 \pm 9.4\%$ according to
 312 the RTE model. In this case, identification is not possible; others measurements
 313 and/or another radiative models are needed to ensure the well-posed character
 314 of the inverse problem.

315 These examples illustrate how SMC allows to determine the existence, unic-
 316 ity and stability of the inverse problem solution.

317 3.5. Application to a Quartzel sample

318 Once the spectral range where the absorption and scattering coefficients
 319 identification is feasible has been determined from SMC analysis, the inverse
 320 procedure can be applied. Identification of κ_η and σ_η at a wavenumber η is
 321 performed from measurements of transmittance and reflectance and from SMC
 322 polynomials. Here, a Levenberg-Marquardt algorithm is used to determine κ_η
 323 and σ_η .

324 In the inverse procedure, the two polynomials corresponding to transmit-
 325 tance and reflectance are used as direct model for radiation, and avoid the
 326 costly resolution of the RTE at each wavenumber, and each iteration of the
 327 inversion algorithm. Thus, only one SMC simulation is carried out during the
 328 inverse method, which decreases significantly the computational cost.

329 Identified absorption and scattering coefficients are plotted in figure 8. Error
 330 bars of identified κ_η and σ_η in figure 8 are determined based on the principle
 331 described in figure 7. They correspond to the minimum and maximum value
 332 of the admissible zone with an experimental uncertainty of ± 0.01 which is the
 333 maximal value of calculated experimental uncertainty over the whole spectrum.
 334 SMC analysis showed that the identification of radiative properties is impossible

335 for wavenumbers in the intervals [700; 870] and [950; 1245] cm^{-1} . These spectral
336 regions are depicted in grey in figure 8. In these regions, measured transmittance
337 is lower than 0.01. It ranges within the detector internal noise which leads to
338 a relative uncertainty of 100%. In this particular case, the range of possible
339 absorption and scattering coefficients that are solutions of the inverse problem
340 are unbounded as it was illustrated in figure 7b. The medium is optically thick
341 and the RTE model turns out to be unsuitable for the identification at these
342 wavenumbers. SMC showed that the identification of radiative properties is
343 possible in other spectral regions *i.e.*, [870; 950] and [1245; 3700] cm^{-1} .

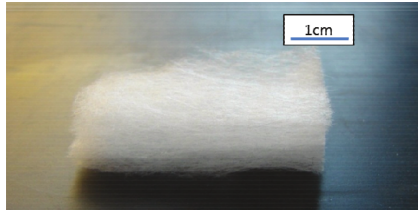
344 4. Conclusion

345 In the present work, SMC was applied to express directional-hemispherical
346 transmittance and reflectance as polynomials of absorption and scattering co-
347 efficients. An analysis based on these polynomials allows to determine if the
348 radiative properties identification is feasible or not, illustrating the well or ill-
349 posed nature of the inverse problem. Indeed, the contour intersection approach
350 shows if the solution exists and is unique, and an analysis based on experimen-
351 tal and numerical uncertainties shows if the solution is reliable or not. When
352 identification is feasible, SMC polynomials combined with an optimization algo-
353 rithm allows to retrieve the range of absorption and scattering coefficients that
354 are solutions of the inverse problem. The approach has been applied to identify
355 the radiative properties of a heterogeneous material, a Quartzel low-density felt.
356 Using the SMC polynomials as direct model in the inverse iterative procedure,
357 the RTE is only solved once with SMC. The numerical efficiency is therefore
358 significantly improved.

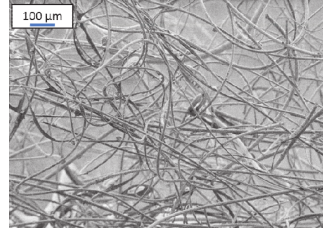
359 The method proposed in this paper can be applied to other kind of materials
360 with different structure, density and porosity to identify potential limits of SMC.
361 Moreover, it can also be applied to phase function parameters identification if bi-
362 directional measurements are carried out. Indeed, SMC can be used to express
363 radiative quantities as polynomials of absorption and scattering coefficients, as

364 well as phase function parameters [17]. The SMC polynomials would then allow
365 the identification of phase function (in addition to absorption and scattering
366 coefficients).

367 In future works, the identification of radiative properties of materials at high
368 temperature from spectroscopic emission measurements will be investigated.
369 The experimental bench described in [18] will be used. The development of an
370 efficient identification strategy at high temperature remains a challenging task
371 since the ill-posed character of the inverse problem has been highlighted in [19]
372 when the RTE model is chosen. The SMC framework proposed in this work will
373 be developed further in order to guide inverse modeling in this context.



(a)



(b)

Figure 1: (a) Example of a Quartzel sample. (b) Scanning Electron Microscope (SEM) picture of Quartzel. Pictures from [20]

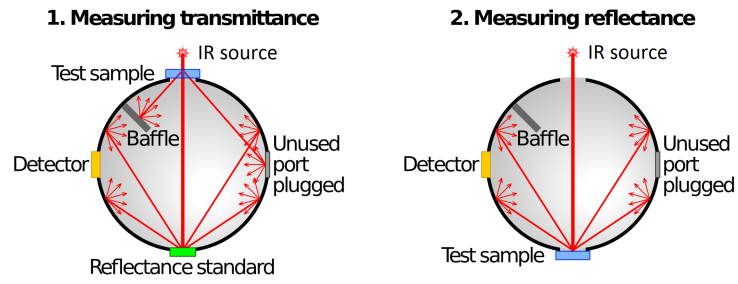


Figure 2: Integrating sphere configurations for transmittance and reflectance

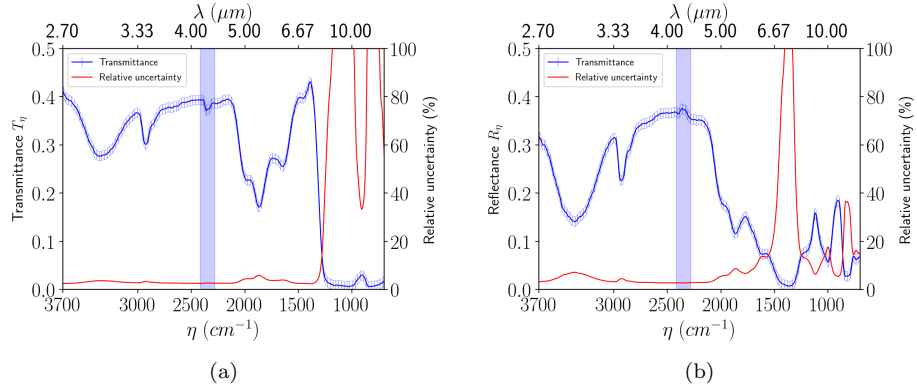


Figure 3: Mean measurements of (a) transmittance and (b) reflectance with their associated uncertainties. The colored blue band corresponds to CO_2 absorption band between $\eta = 2222$ and $\eta = 2398 \text{ cm}^{-1}$ where measurements are not taken into account.

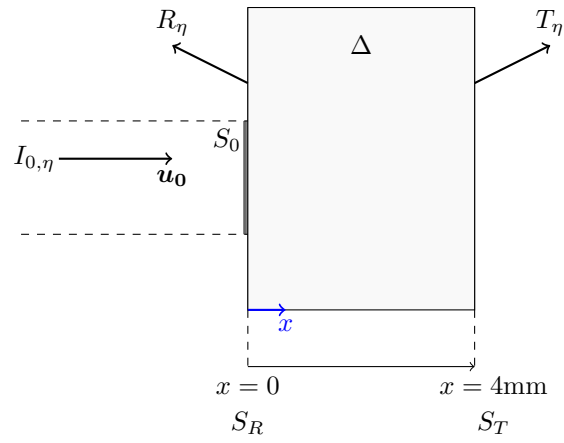


Figure 4: Representation of the sample in a configuration of directional-hemispherical measurement of transmittance and reflectance.

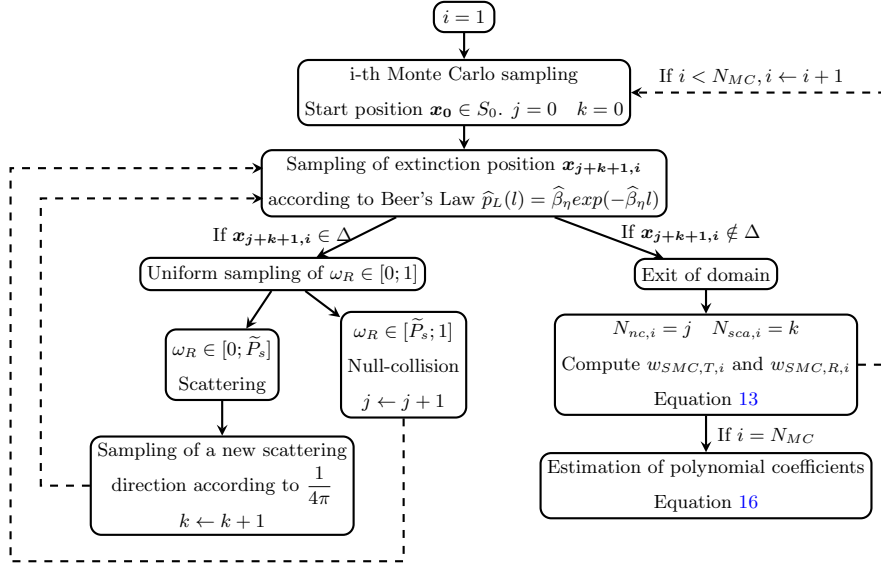


Figure 5: Symbolic Monte Carlo algorithm for the estimation of directional-hemispherical transmittance and reflectance

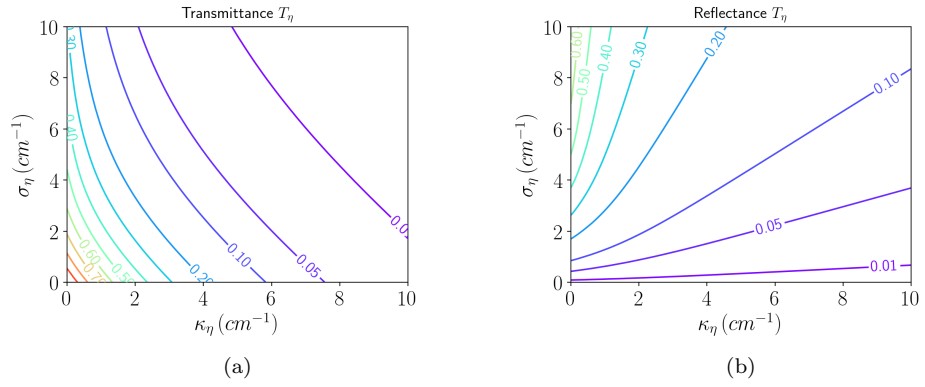


Figure 6: Isovalues of directional-hemispherical (a) transmittance T_η and (b) reflectance R_η computed with SMC as a function of absorption and scattering coefficients

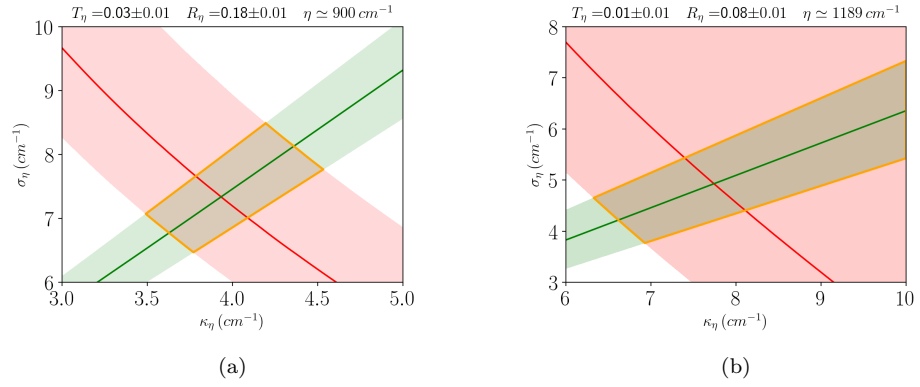


Figure 7: Region of possible solution κ_η and σ_η at (a) $\eta = 900 \text{ cm}^{-1}$ and (b) $\eta = 1189 \text{ cm}^{-1}$, when experimental and numerical uncertainties are included in the analysis.

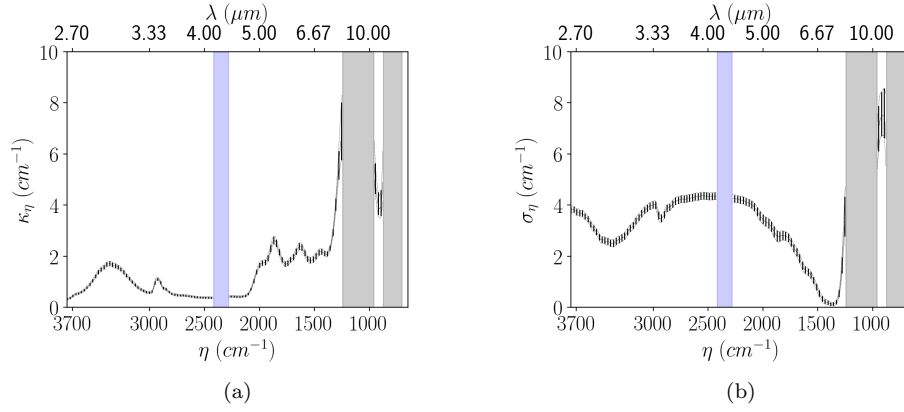


Figure 8: Identified (a) absorption and (b) scattering coefficients using SMC polynomials and taking into account measurements uncertainties. Colored band (in blue) in spectral range $[2222; 2398] \text{ cm}^{-1}$ ($[4.17; 4.5] \mu\text{m}$) represents absorption peak by CO_2 absorption. Grey bands display spectral ranges where the identification is not feasible.

374 **Appendix A. Consequences of the arbitrary choice of \widetilde{P}_s on SMC**
 375 **standard-deviation**

376 With SMC, standard-deviation can be expressed as a polynomial of absorp-
 377 tion and scattering coefficients [12]:

$$\begin{aligned} \text{SSMC}(T_\eta(\kappa_\eta, \sigma_\eta)) = & \left[\frac{1}{N_{MC} - 1} \sum_{j=0}^{\infty} \sum_{k=0}^{\infty} \sum_{j'=0}^{\infty} \sum_{k'=0}^{\infty} (\overline{a_{jk} a_{j'k'}} - \overline{a_{jk}} \overline{a_{j'k'}}) \right. \\ & \left. \times \left(\frac{\widehat{\beta}_\eta - \kappa_\eta - \sigma_\eta}{\widehat{\beta}_\eta(1 - \widetilde{P}_s)} \right)^{j+j'} \left(\frac{\sigma_\eta}{\widehat{\beta}_\eta \widetilde{P}_s} \right)^{k+k'} \right]^{1/2} \end{aligned} \quad (\text{A.1})$$

where:

$$\overline{a_{jk} a_{j'k'}} = \frac{1}{N_{MC}} \sum_{i=1}^{N_{MC}} (a_{jk,i} a_{j'k',i}) \quad (\text{A.2})$$

378 and $a_{jk,i}$ are given by Eq 14 and $\overline{a_{jk}}$ by Eq 16.

379 Under pure statistical considerations, such functional expressions of standard-
 380 deviations present a valuable advantage: the evolution of the uncertainty with
 381 the considered parameters is explicit, and may provide relevant information on
 382 the definition of the arbitrary probability \widetilde{P}_s .

383 In the algorithm described in subsection 3.3, absorption and scattering coeffi-
 384 cients are unknown and arbitrary probabilities of scattering \widetilde{P}_s and null-collision
 385 $\widetilde{P}_n = 1 - \widetilde{P}_s$ are required. The introduction of an arbitrary probability does not
 386 create any bias as an infinity of Monte Carlo samples would lead to an exact
 387 solution, but may have significant influence on the statistical uncertainties, and
 388 therefore the convergence speed can be altered. However, in order to ensure a
 389 small standard deviation, arbitrary scattering probability should be consistent
 390 with the statistics of the considered physics [12] and should be close to the ratio
 391 of the number of scattering events over the whole number of collisions given by
 392 equation 5.

393 The influence of this choice is illustrated in figure A.9. Three SMC cal-
 394 culations have been carried out with three different \widetilde{P}_s ($\widetilde{P}_s = 0.2$, $\widetilde{P}_s = 0.5$
 395 and $\widetilde{P}_s = 0.8$) with $N_{MC} = 10^6$. The three estimated SMC relative standard-
 396 deviation are compared over the spectrum. For $\widetilde{P}_s = 0.5$, used in this work,

397 relative standard-deviation has a maximum value of 2.1% for transmittance and
 398 2.6% for reflectance which is satisfactory for the identification of absorption and
 399 scattering coefficient. If \widetilde{P}_s is taken equal to 0.2, maximum relative standard-
 400 deviation observed over the spectrum is 0.6% for transmittance and 0.3% for
 401 reflectance. However, if $\widetilde{P}_s = 0.8$, maximum relative standard-deviation ob-
 402 served over the spectrum is close to 40% for transmittance and reflectance. For
 403 the studied sample, the best choice of \widetilde{P}_s would have been 0.2 since it is the
 404 closest to the real value of $P_{s,\eta} = \frac{\sigma_\eta}{\widehat{\beta} - \kappa_\eta}$ in the most part of the spectrum.

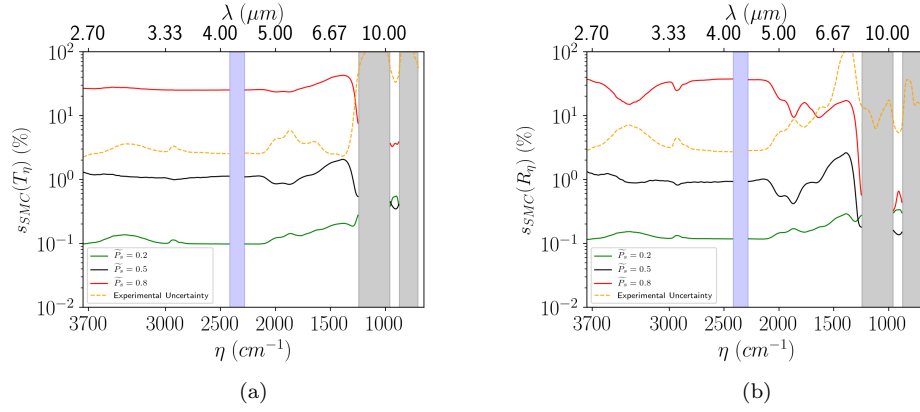


Figure A.9: Relative standard-deviation estimated using SMC for (a) transmittance and (b) reflectance, for different values of \tilde{P}_s .

405 **References**

- 406 [1] D. Baillis, M. Arduini-Schuster, J. Sacadura, Identification of spectral
407 radiative properties of polyurethane foam from hemispherical and bi-
408 directional transmittance and reflectance measurements, *Journal of Quan-*
409 *titative Spectroscopy and Radiative Transfer* 73 (2002) 297 – 306. doi:
410 [https://doi.org/10.1016/S0022-4073\(01\)00199-6](https://doi.org/10.1016/S0022-4073(01)00199-6).
- 411 [2] J. Sacadura, D. Baillis, Experimental characterization of thermal radiation
412 properties of dispersed media, *International Journal of Thermal Sciences*
413 41 (2001) 699 – 707. doi:[https://doi.org/10.1016/S1290-0729\(02\)](https://doi.org/10.1016/S1290-0729(02)01365-0)
414 [01365-0](https://doi.org/10.1016/S1290-0729(02)01365-0).
- 415 [3] T. Ren, M. F. Modest, A. Fateev, S. Clausen, An inverse radiation model
416 for optical determination of temperature and species concentration: Devel-
417 opment and validation, *Journal of Quantitative Spectroscopy and Radiative*
418 *Transfer* 151 (2015) 198 – 209. doi:[https://doi.org/10.1016/j.jqsrt.](https://doi.org/10.1016/j.jqsrt.2014.10.005)
419 [2014.10.005](https://doi.org/10.1016/j.jqsrt.2014.10.005).
- 420 [4] T. Tarvainen, V. Kolehmainen, S. R. Arridge, J. P. Kaipio, Image recon-
421 struction in diffuse optical tomography using the coupled radiative trans-
422 portdiffusion model, *Journal of Quantitative Spectroscopy and Radiative*
423 *Transfer* 112 (16) (2011) 2600 – 2608. doi:[https://doi.org/10.1016/j.](https://doi.org/10.1016/j.jqsrt.2011.07.008)
424 [jqsrt.2011.07.008](https://doi.org/10.1016/j.jqsrt.2011.07.008).
- 425 [5] A. Addoum, O. Farges, F. Asllanaj, Optical properties reconstruction using
426 the adjoint method based on the radiative transfer equation, *Journal of*
427 *Quantitative Spectroscopy and Radiative Transfer* 204 (2018) 179 – 189.
428 doi:<https://doi.org/10.1016/j.jqsrt.2017.09.015>.
- 429 [6] A. Tilioua, L. Libessart, G. Jeandel, S. Lassue, Determination of ra-
430 diative properties of polyester batting insulation material from hemi-
431 spherical transmittance and reflectance measurements, *Applied Thermal*
432 *Engineering* 105 (2016) 594 – 604. doi:[https://doi.org/10.1016/j.](https://doi.org/10.1016/j.applthermaleng.2016.03.050)
433 [applthermaleng.2016.03.050](https://doi.org/10.1016/j.applthermaleng.2016.03.050).

- 434 [7] P. Boulet, J. Grardin, Z. Acem, G. Parent, A. Collin, Y. Pizzo, B. Porterie,
435 Optical and radiative properties of clear PMMA samples exposed to a ra-
436 diant heat flux, *International Journal of Thermal Sciences* 82 (2014) 1–8.
437 [doi:https://doi.org/10.1016/j.ijthermalsci.2014.03.013](https://doi.org/10.1016/j.ijthermalsci.2014.03.013).
- 438 [8] A. Milandri, F. Asllanaj, G. Jeandel, Determination of radiative properties
439 of fibrous media by an inverse methodcomparison with the Mie theory,
440 *Journal of Quantitative Spectroscopy and Radiative Transfer* 74 (2002)
441 637 – 653. [doi:https://doi.org/10.1016/S0022-4073\(01\)00276-X](https://doi.org/10.1016/S0022-4073(01)00276-X).
- 442 [9] W. Dunn, J. Shultis, *Exploring Monte Carlo Methods*, Elsevier Science &
443 Technology, 2011.
- 444 [10] W. Dunn, Inverse Monte Carlo solutions for radiative transfer in inhomoge-
445 neous media, *Journal of Quantitative Spectroscopy and Radiative Trans-*
446 *fer* 29 (1983) 19 – 26. [doi:https://doi.org/10.1016/0022-4073\(83\)](https://doi.org/10.1016/0022-4073(83)90141-3)
447 [90141-3](https://doi.org/10.1016/0022-4073(83)90141-3).
- 448 [11] S. Subramaniam, P. Menguc, Solution of the inverse radiation problem for
449 inhomogeneous and anisotropically scattering media using a Monte Carlo
450 technique, *International Journal of Heat and Mass Transfer* 34 (1991) 253
451 – 266. [doi:https://doi.org/10.1016/0017-9310\(91\)90192-H](https://doi.org/10.1016/0017-9310(91)90192-H).
- 452 [12] M. Galtier, M. Roger, F. André, A. Delmas, A symbolic approach for the
453 identification of radiative properties, *Journal of Quantitative Spectroscopy*
454 *and Radiative Transfer* 196 (2017) 130 – 141. [doi:https://doi.org/10.](https://doi.org/10.1016/j.jqsrt.2017.03.026)
455 [1016/j.jqsrt.2017.03.026](https://doi.org/10.1016/j.jqsrt.2017.03.026).
- 456 [13] M. Galtier, S. Blanco, C. Caliot, C. Coustet, J. Dauchet, M. E. Hafi,
457 V. Eymet, R. Fournier, J. Gautrais, A. Khuong, B. Piaud, G. Terre,
458 Integral formulation of null-collision Monte Carlo algorithms, *Journal of*
459 *Quantitative Spectroscopy and Radiative Transfer* 125 (2013) 57 – 68.
460 [doi:https://doi.org/10.1016/j.jqsrt.2013.04.001](https://doi.org/10.1016/j.jqsrt.2013.04.001).

- 461 [14] P. Honnerová, J. Martan, Z. Veselý, M. Honner, Method for emissivity
462 measurement of semitransparent coatings at ambient temperature, Scien-
463 tific Reports 7. doi:<https://doi.org/10.1038/s41598-017-01574-x>.
- 464 [15] V. Eymet, D. Poitou, M. Galtier, M. E. Hafi, G. Terre, R. Fournier, Null-
465 collision meshless Monte Carlo : Application to the validation of fast ra-
466 diative transfer solvers embedded in combustion simulators, Journal of
467 Quantitative Spectroscopy and Radiative Transfer 129 (2013) 145 – 157.
468 doi:<https://doi.org/10.1016/j.jqsrt.2013.06.004>.
- 469 [16] B. Sumlin, W. Heinson, R. Chakrabarty, Retrieving the aerosol complex
470 refractive index using pymiescatt: A Mie computational package with visu-
471 alization capabilities, Journal of Quantitative Spectroscopy and Radiative
472 Transfer 205 (2018) 127 – 134. doi:[https://doi.org/10.1016/j.jqsrt.](https://doi.org/10.1016/j.jqsrt.2017.10.012)
473 [2017.10.012](https://doi.org/10.1016/j.jqsrt.2017.10.012).
- 474 [17] M. Roger, Y. Maanane, M. Galtier, F. André, A. Delmas, Symbolic Monte
475 Carlo method based on orthogonal polynomial series: application to phase
476 function, 2019. doi:[10.1615/RAD-19.360](https://doi.org/10.1615/RAD-19.360).
- 477 [18] S. Le Foll, A. Delmas, F. André, Identification of radiative properties
478 for heterogeneous materials at high temperature, International Journal of
479 Thermal Sciences 120 (2017) 314–320. doi:[10.1016/j.ijthermalsci.](https://doi.org/10.1016/j.ijthermalsci.2017.06.019)
480 [2017.06.019](https://doi.org/10.1016/j.ijthermalsci.2017.06.019).
- 481 [19] M. Roger, M. Galtier, F. André, A. Delmas, Symbolic Monte Carlo meth-
482 ods: an analysis tool for the experimental identification of radiative proper-
483 ties at high temperature, Eurotherm Seminar 110 - Computational Thermal
484 Radiation in Participating Media VI at Cascais (Portugal), 2018.
- 485 [20] N. Diascorn, [Elaboration and characterization of silica and polyurethane](#)
486 [based thermal superinsulating hybrid aerogels](#), Phd thesis, Ecole Nationale
487 Supérieure des Mines de Paris (Dec 2014).
488 URL <https://pastel.archives-ouvertes.fr/tel-01151554>